FOCUSED ISSUE FEATURE

Promising Future of Metamaterials

Yuandan Dong and Tatsuo Itoh

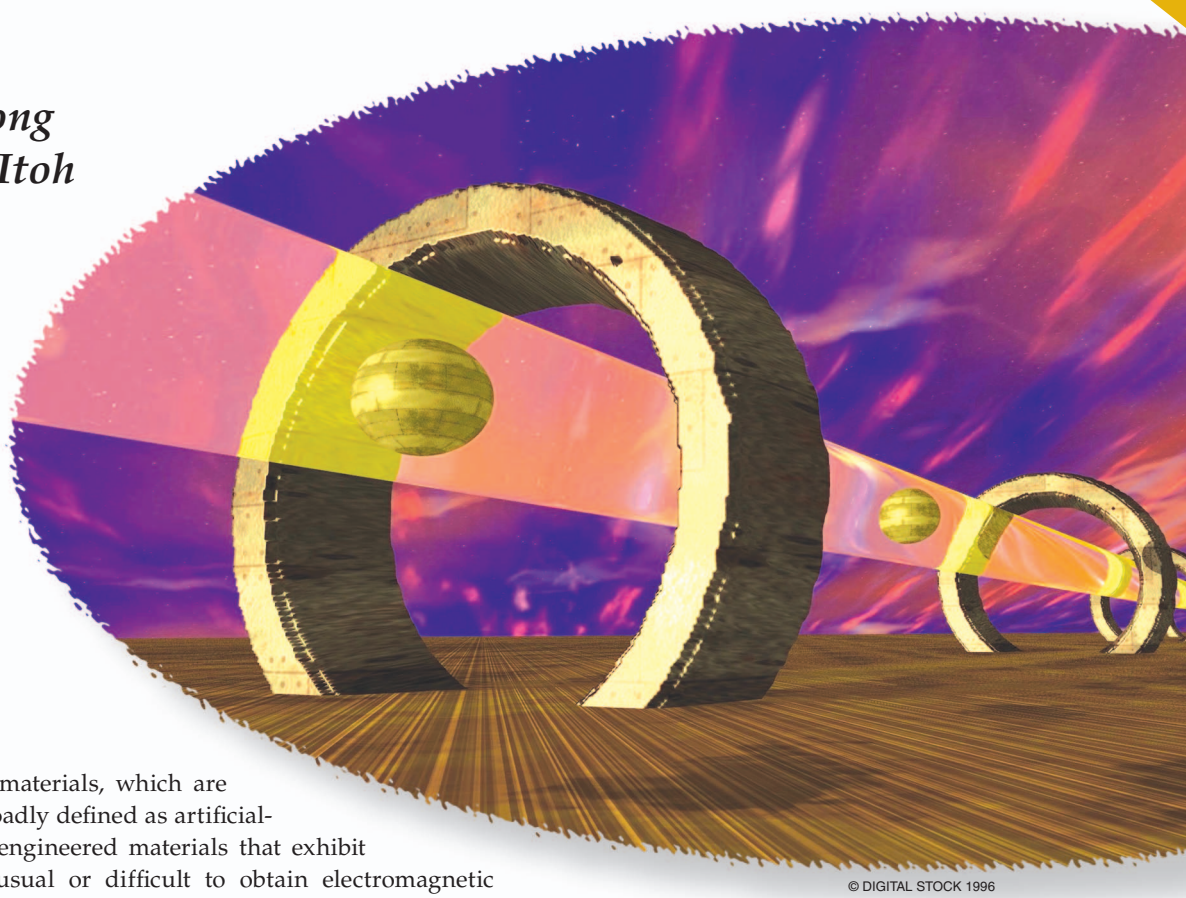

Metamaterials, which are broadly defined as artificially engineered materials that exhibit unusual or difficult to obtain electromagnetic (EM) properties, have spurred a significant research interest over the past decade [1]–[6]. They are explained in the general context of periodical structures with a periodicity that is much smaller than the guided wavelength. Their exotic properties include negative or low values of permittivity (ε), permeability (μ), and refractive index (n), which are not readily available from conventional materials. These properties have enabled the development of new concepts and devices and possible utilization in many novel applications [1]–[6]. For instance, metamaterials with simultaneously negative permittivity and permeability are referred to as left-handed (LH) materials [1]. By including the right-handed (RH) effects that occur naturally in traditional materials, a more general model has been proposed as composite right/left-handed (CRLH) structures [2], [7]. Strictly speaking, all the practical LH media actually falls under the designation of CRLH materials since their left-handedness only holds in a small frequency band. In some scenarios, the RH region is just too far away, thus not in the region of interest. The classification of materials can be graphically illustrated with the $\varepsilon-\mu$ diagram shown in Figure 1. It should be pointed out that only the double-positive medium and double-negative medium allow the wave propagation while the single negative materials prohibit the wave transmission. The double-negative

Yuandan Dong (yddong@ee.ucla.edu) and Tatsuo Itoh (itoh@ee.ucla.edu) are with the Electrical Engineering Department, 63-129 ENGR-IV, University of California at Los Angeles, Los Angeles, CA 90095, USA.

Digital Object Identifier 10.1109/MMM.2011.2181447
Date of publication: 9 March 2012

Strictly speaking, all the practical LH media actually falls under the designation of CRLH materials since their left-handedness only hold in a small frequency band.

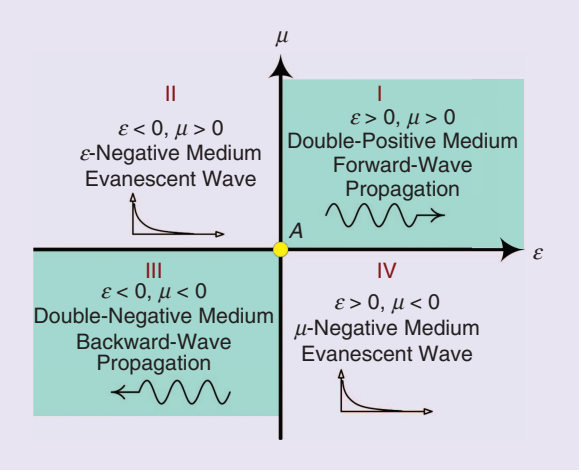

Figure 1. *The permittivity-permeability* $(\varepsilon-\mu)$ *diagram which shows the material classifications. At the intersection (point A) it is the zero-index media.*

medium (LH material) is characterized by antiparallel phase and group velocities, negative refractive index (NRI), and backward-wave propagation, which differs from the RH material. It is also noted that at the intersection of the various types of materials, there is the zero-index media as indicated by Figure 1. Owing to its infinite wavelength propagation, the zero-index metamaterial offers some interesting features and applications that have drawn some special attention in the community [2], [4], [7]–[9]. Metamaterials have provided the engineers with a means to manipulate the material's intrinsic parameters so as to control and utilize the propagation of EM waves.

In this article, we focus on the waveguide structures loaded with metamaterial elements, especially their wave propagation characteristics and the practical applications for guided and radiated microwave components. Here we mainly consider the waveguide with transverse electric (TE) or transverse magnetic (TM) propagation modes. Due to the difficulty in accurately extracting the equivalent circuit from the waveguide structures, especially after inserting the metamaterial loadings, this article mainly discusses their properties from the point of view of materials in terms of the permittivity and permeability. It is noted that they may also have other interpretations from different engineering angles. For instance, we can still analyze them using the equivalent circuits as we did in several previous papers. We can also use the periodic structures or coupled resonator theory from filter synthesis point of view for analysis and design. These different approaches do not conflict and eventually should achieve the same design purpose and results.

Basic Types of Metamaterial Elements

The most original and well-known LH material was proposed by a group in the University of California at San Diego (USCD) [1]. It consists of the split-ring resonators (SRRs) and thin copper wires, providing the negative permeability and negative permittivity, respectively. The SRRs behave similarly to the resonant magnetic dipoles which can be excited by an axial magnetic field [10], [11]. In 2004, from a duality argument, complementary SRRs (CSRRs) were introduced by Falcone et al. as new metamaterial elements and have been proven to exhibit negative permittivity [12]. It is noted that the thin copper wire can be considered as an electric dipole. It also has a dual counterpart, which is the slot magnetic dipole. The slot has been used to synthesize transmission line (TL) metamaterials and provides the LH capacitance instead of the consideration of a magnetic dipole. Essentially, they function in the same way, and sometimes the slot is meandered in order to increase its effective length. Figure 2 summarizes all four metamaterial elements above, which can be considered as two pairs of electric and magnetic dipoles.

It is important to bear in mind that both permittivity and permeability are tensors and only one of the tensor components could be thought to be negative for the artificial metamaterials synthesized by elements shown in Figure 2. Specifically, for the orientations shown in the figure, they can be described as

$$\bar{\varepsilon} = \begin{bmatrix} \varepsilon_{xx} & 0 & 0 \\ 0 & \varepsilon_{yy} & 0 \\ 0 & 0 & \varepsilon_{zz} \end{bmatrix} = \varepsilon_0 \begin{bmatrix} \varepsilon_{\mathrm{lr}} & 0 & 0 \\ 0 & \varepsilon_{\mathrm{lr}} & 0 \\ 0 & 0 & \varepsilon_{\mathrm{tr}} \end{bmatrix} = \varepsilon_0 \, \bar{\varepsilon}_r, \quad (1)$$

$$\bar{\mu} = \begin{bmatrix} \mu_{xx} & 0 & 0 \\ 0 & \mu_{yy} & 0 \\ 0 & 0 & \mu_{zz} \end{bmatrix} = \mu_0 \begin{bmatrix} \mu_{\mathrm{lr}} & 0 & 0 \\ 0 & \mu_{\mathrm{tr}} & 0 \\ 0 & 0 & \mu_{\mathrm{lr}} \end{bmatrix} = \mu_0 \, \bar{\mu}_r, \quad (2)$$

where ε_0 and μ_0 are the free space permittivity and permeability, $\varepsilon_{\mathrm{tr}}(\mu_{\mathrm{tr}})$ and $\varepsilon_{\mathrm{lr}}(\mu_{\mathrm{lr}})$ are the relative permittivity (permeability) in the transversal and longitudinal directions, and $\varepsilon_{\mathrm{tr}}$ and μ_{tr} could be negative for the displayed elements in Figure 2.

Most of the available metamaterial structures, except the lumped element type [13] and waveguide-based metamaterials [14]–[17], are synthesized based on these elements. On the other hand, arbitrarily selecting two of them (one electric dipole and one magnetic dipole) could usually result in a metamaterial realization once they are properly oriented. Specifically, there are four combination methods as shown below.

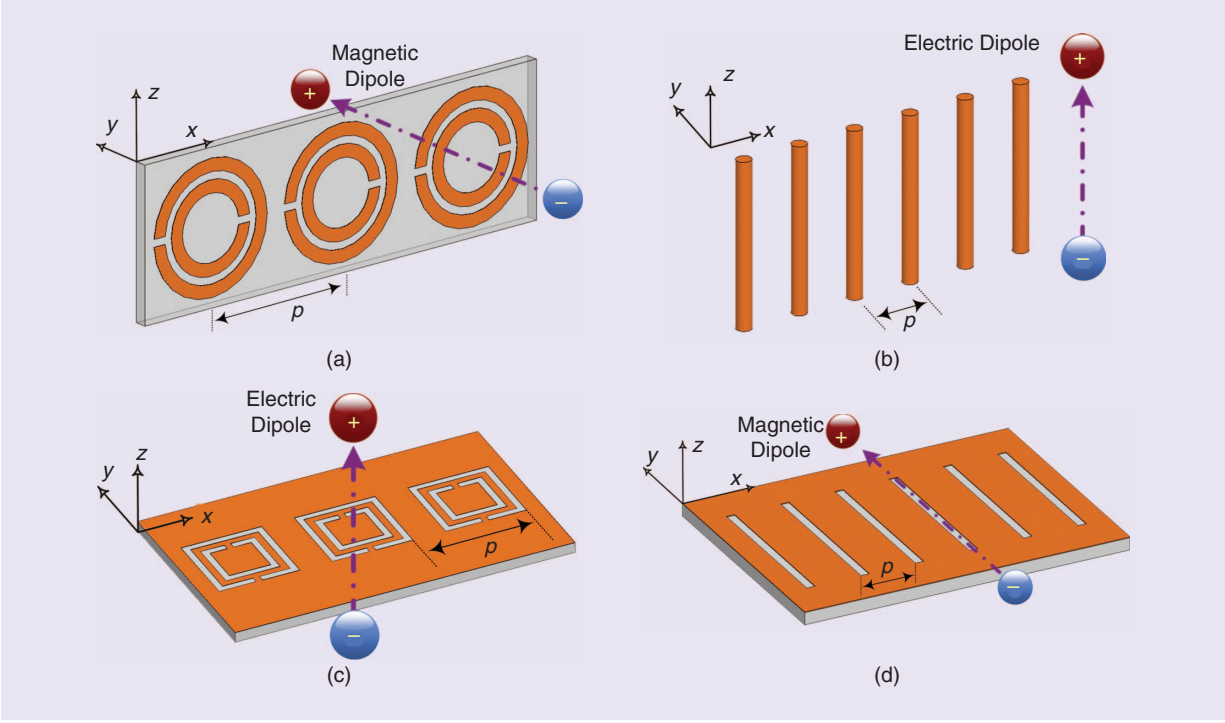

Figure 2. *A summary of the different metamaterial elements that have been used for metamaterial synthesis: (a) SRRs, which can be considered as equivalent magnetic dipoles, (b) metal wire lines, which are regarded as electric dipoles, (c) CSRRs, which are considered as equivalent electric dipoles, and (d) slot lines, which can be viewed as magnetic dipoles.*

- *SRR and Wire dipole*: this case is the most original and widely used combination mode [1].
- *SRR and CSRR*: one realizing example using SRR and CSRR is shown in [18]. Due to the difficulty in arrangement, this combination mode does not gain much popularity.
- *Slot dipole and wire dipole*: The mushroom structure as shown in Figure 3(a) falls into this configuration [19], [20]. The mushroom structure was first proposed by Sievenpiper et al. in [19] for the realization of high-impedance surfaces. Many papers have investigated this structure using the CRLH TL theory [8], [9]. In essence, the coupling slots can be considered as slot dipoles providing the negative μ, while the vias can be viewed as wire dipoles which exhibit a negative ε.
- *Slot dipole and CSRR*: One example is shown in Figure 3(b) [21]. This combination mode is widely employed in microstrip technology [11].

Note that different configurations listed above could result in varied performances. Generally speaking, the TL metamaterials based on the CRLH theory are capable of providing a wider bandwidth compared with the resonator-type metamaterials. Nevertheless, those structures are considered lossy therefore inefficient. One way to increase the efficiency is to switch to the waveguide structures, which provide a much higher quality (Q) factor.

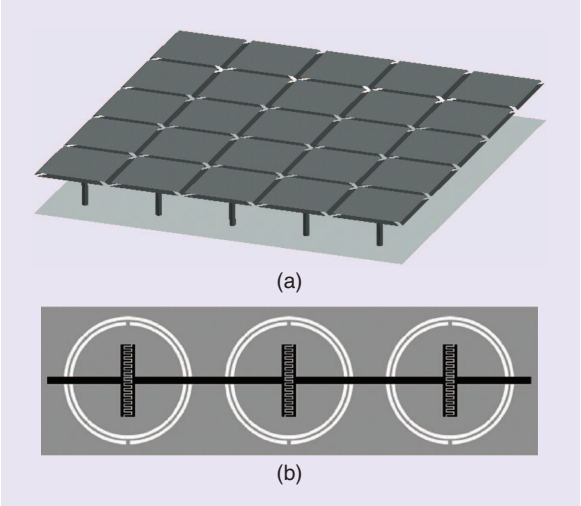

Figure 3. *(a) Mushroom structure, which consists of coupling slots and vias connected to the ground. It has been demonstrated to be a CRLH structure with an NRI [20]. (b) Planar CRLH structure for composed by interdigital coupling slots and CSRRs on the ground. It has been used for wideband filter applications [21].*

Waveguide Loaded with Metamaterials

A question arises: why do we choose waveguide structures to apply the metamaterials? One reason as stated above is that waveguide exhibits a high Q-factor which could be utilized to design low loss components with a good power handling capability. The second reason is

that the waveguide is able to provide negative permittivity when operated below the cutoff frequency of the dominant TE mode [14]. It is well-known that rectangular waveguide can support TE and TM modes with the dispersion constant satisfying the following relation [22]

$$k = \omega\sqrt{\mu_r\,\varepsilon_{\text{eff}}},\quad \varepsilon_{\text{eff}} = \varepsilon_r\left(1-\frac{\omega_0^2}{\omega^2}\right), \tag{3}$$

where μ_r and ε_r are the permeability and permittivity of the substrate filling inside the waveguide, and ω_0 is the cutoff frequency for the considered mode. When the waveguide is operated below the cutoff frequency, ε_{eff} becomes negative and k becomes an imaginary number. The resulting mode is an evanescent one where the wave propagation is prohibited. It falls into the ε-negative material corresponding to second quadrant of the ε-μ diagram shown in Figure 1. This feature seems to be pointless to normal waveguide applications while it becomes an extremely attractive property under the scenario of metamaterial synthesis. We automatically obtain a uniform ε-negative material without introducing any resonant structures or any additional loss for the frequency range below the waveguide cutoff [14]. It should be pointed out the traditional wire arrays, which also follow the Drude model, can also be used to achieve a nonresonant ε-negative medium [4], and the use of waveguides below the cutoff is just one of the options which we believe is superior in terms of simplicity and loss.

Waveguide with SRR Loading

One perceptual intuition is that the negative permeability is missing and we only need to introduce a negative-μ material in order to simulate an LH metamaterial in waveguide format. Based on this idea, SRRs are inserted into the waveguide and are placed perpendicularly to the magnetic field in order to facilitate the excitation [14], [15]. The configuration of the unit-cell, which was originally proposed in [14], is displayed in Figure 4. We re-simulated the structure and found a good agreement with the conclusion made in [14]. The propagation curves indicate that there is an LH passband generated around 6.25 GHz where backward-wave propagation can be envisioned as suggested by the dispersion curve. Note that the waveguide cutoff frequency occurs at around 24 GHz. The calculated permittivity and permeability based on *S*-parameters verify that it is a double negative material inside the interested frequency range. The refractive index clearly demonstrates that it is a one-dimensional NRI material and phase advance (positive phase) occurs in the passband.

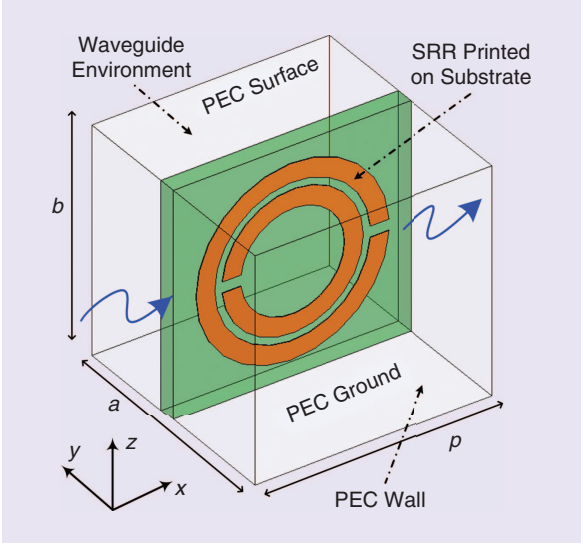

Figure 4. *SRR-loaded waveguide unit-cell that was originally proposed in [14] in order to excite an LH passband below the waveguide cutoff frequency. It is proven to exhibit negative μ and negative ε inside the LH passband, which come from the below-cutoff operation and the SRR, respectively [14].*

Waveguide with CSRR Loading

Since the CSRR also exhibits negative permittivity, it would be interesting to investigate the case of incorporating CSRRs into the waveguide. Would the combination of two ε-negative materials give rise to a ε-positive material? We simulated the unit-cell of this structure which is shown in Figure 5(a) [23]. Two CSRRs are face-to-face oriented in terms of the split direction and incorporated on the waveguide surface. It is noted that all the simulation performed here is based on Ansoft's High Frequency Structure Simulator (HFSS) software package. Then we retrieved all the material parameters using the simulated *S*-parameters [24]. The results are displayed in Figure 5(b)–(d). Figure 5(b) shows the dispersion curve and attenuation constant which demonstrates that a forward-wave passband below the cutoff is achieved around 4.8 GHz. For this configuration the waveguide cutoff frequency is at about 9.8 GHz. Figure 5(c) confirms our assumption that positive permittivity is obtained inside this passband. It is interesting to see that by loading an ε-negative material into the waveguide we can manipulate the original material parameters resulting in a forward-wave passband far below the waveguide cutoff, which is very suitable to be utilized for real applications. We can explain this phenomenon in this way: first it is well known that a microstrip line or a parallel-plate waveguide loaded with CSRRs provides an equivalent ε-negative medium [12]. Then we create a waveguide environment and operate it below the cutoff frequency. According to (3), since the original ε_r is negative, the resulting ε_{eff} becomes positive for the frequency below ω_0. It can also be interpreted in the way that CSRR is able to reverse the permittivity of the original material. Therefore initial ε-negative material below the waveguide cutoff becomes ε-positive after inserting the CSRRs. Figure 5(d) plots the phase response and refractive index which indicates that this passband has a negative phase (phase delay)

and positive index. Outside the passband region below the cutoff, it is considered as single-negative material (ε-negative and μ-positive) corresponding to the stopband. The obtained refractive index, as defined by (4) [2], becomes imaginary and meaningless. It is noted that we still consider this structure for metamaterial applications in such a way we employ a metamaterial structure to engineer the effective material parameters and facilitate the wave propagation which is not easily attainable with traditional technology like the evanescent wave propagation by inserting capacitive nontouching fins or post [25], [26].

$$n = \pm\sqrt{\varepsilon_r \mu_r}. \tag{4}$$

Waveguide with Slot-Line Loading

Now we discuss the third case, where the waveguide is loaded by slot dipoles etched on the top surface. The unit-cell configuration is shown in Figure 6(a). To increase the effective slot length, we modified the original slot to a meander type slot line. Based on the simulated S-parameters, we extracted the dispersion curve and material parameters as shown in Figure 6(b)–(d) [27]. Figure 6(b) shows that a balanced condition is achieved where the LH region and the RH region are seamlessly connected. Note that this is optimized results. Otherwise a bandgap would appear between the two regions. The attenuation characteristic indicates that a very broad passband is achieved starting from 8 GHz to 14 GHz. The transition frequency is designed to be 10 GHz. Figure 6(c) shows the calculated material parameters. The phase response and refractive index are plotted in Figure 6(d). It is seen that with the increase of the frequency, the material changes from double-negative medium, to zero-index medium, and finally to double-positive medium. In the LH region, phase advance occurs while phase delay happens in the RH region. At the transition frequency, the wavelength goes to infinity. Different from the above two cases, this design is able to offer a very wide operating bandwidth. We can also use the CRLH concept to analyze the structure and the related equivalent circuit is plotted on the right side of Figure 6(a) [27], [28]. Its dispersion relation can be determined as [2]

$$\beta(\omega) = \frac{1}{p}\cos^{-1}\left(1 - \frac{1}{2}\left(\frac{\omega_L^2}{\omega^2} + \frac{\omega^2}{\omega_R^2} - \frac{\omega_L^2}{\omega_{se}^2} - \frac{\omega_L^2}{\omega_{sh}^2}\right)\right), \tag{5}$$

where p is the length of the unit-cell and

$$\omega_L = \frac{1}{\sqrt{C_L L_L}}, \quad \omega_R = \frac{1}{\sqrt{C_R L_R}},$$

$$\omega_{se} = \frac{1}{\sqrt{C_L L_R}}, \quad \omega_{sh} = \frac{1}{\sqrt{C_R L_L}}.$$

There are two frequency points that are referred to as the infinite wavelength points ($\beta = 0$) with a bandgap

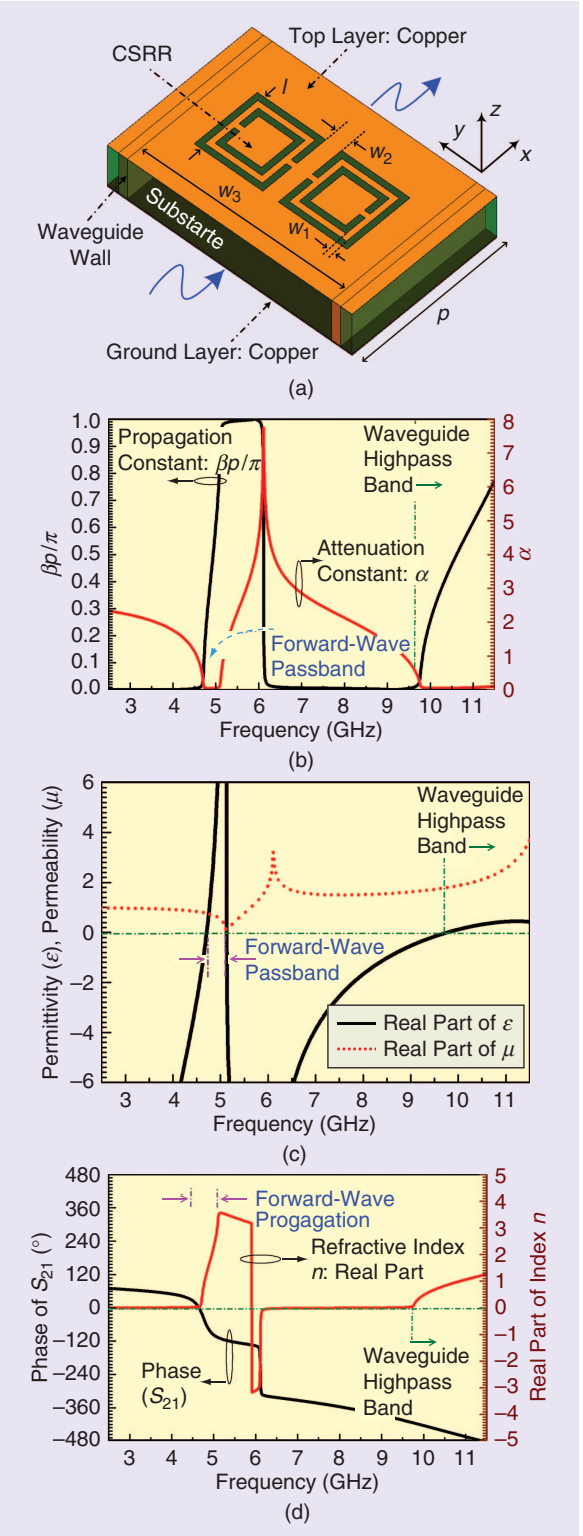

Figure 5. *CSRR-loaded waveguide unit-cell and its characters. This structure was originally proposed and investigated in [23] for the purpose of miniaturized filter design. (a) Configuration, (b) simulated dispersion and attenuation constant, (c) calculated effective permittivity and permeability (real part), and (d) phase response and refractive index. (Unit-cell parameters: $w_1 = 0.26$ mm, $w_2 = 0.54$ mm, $w_3 = 11.7$ mm, $p = 8$ mm, $l = 3.92$ mm, substrate dielectric constant is 2.2, thickness is 20-mil.)*

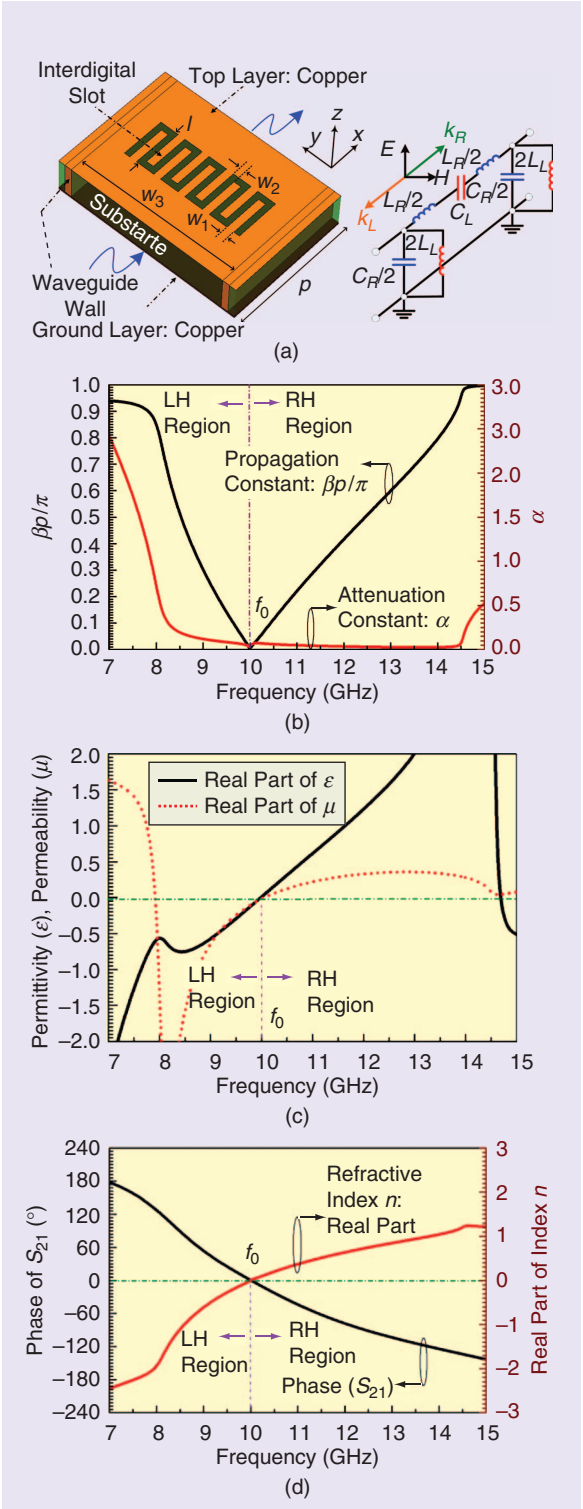

Figure 6. *Interdigital slot-loaded waveguide unit-cell and its features. (a) Configuration and its equivalent circuit, (b) simulated dispersion and attenuation constant, (c) calculated effective permittivity and permeability (real part), and (d) phase response and refractive index. (Unit-cell parameters: $w_1 = 0.33$ mm, $w_2 = 0.45$ mm, $w_3 = 8.84$ mm, $p = 8.2$ mm, $l = 3.3$ mm, substrate dielectric constant is 2.2, and thickness is 20-mil). This structure was originally proposed and analyzed in [24].*

between them. In the balanced case ($\omega_{se} = \omega_{sh}$) they are equal to each other and the bandgap vanishes. Under this scenario choosing interdigital slot is for the purpose of increasing the LH capacitance.

Waveguide with Wire-Line Loading

For the last case of waveguide loaded with wire dipoles, we would just draw a conclusion here. Similarly to the case of waveguide loaded with CSRRs, a forward-wave passband can be generated below the cutoff frequency. The combination of two ε-negative materials leads to a ε-positive operation which enables the wave propagation below the cutoff frequency. The related verification has been presented in [17], [29], where the waveguide miniaturization using wire dipole arrays are proposed. It also gives a relatively broad passband compared with the CSRR-loaded waveguide structures.

Note that there are also other interpretations for the unit-cells and their related transmission characteristics shown above. For instance, the image parameter method is used for periodic structures [22] and the resonance coupling-related wave propagation method is used for the design of evanescent mode waveguide filters [25], [26]. For the latter, backward or forward waves observed in waveguides below cutoff could be caused by interaction between resonators. As we stated before, these different explanations do not conflict as long as they are consistent and justified.

Finally, we also would like to point out that there are still some other metamaterial-based waveguide structures which we did not mention above, for instance, the dielectric resonator based CRLH waveguide structures shown in [30]. Another interesting and important issue we should address is that all of the analysis is based on the TE_{10} mode. When the TM modes are introduced into the waveguide, everything would be reversed and it would provide a μ-negative environment when operated below the cutoff frequency [16]. Under this scenario the electric dipole (such as the CSRRs and wires) loaded waveguide are assumed to offer an LH passband below the cutoff frequency. This is also a potentially rewarding direction for metamaterial application in the waveguide environment.

Microwave Applications

The metamaterial-based waveguide structures have led to many novel microwave devices and applications. This section presents the guided and radiated applications that utilize their unique properties as discussed in the previous section. Since traditional rectangular waveguides are bulky, heavy and it is not very realistic to etch slots on the surface, the substrate integrated waveguide (SIW), which is a new but similar guided wave structure synthesized on the planar substrate with linear periodic arrays of metalized vias, has been chosen in some of the applications

discussed below. Exactly like the rectangular waveguide, the dominant mode of SIW is still TE_{10} mode and it possesses a characteristic cutoff frequency [31], [32]. Half mode SIW (HMSIW), which keeps the half of the field distribution of the dominant TE_{10} mode, reduces the size of conventional SIW structure nearly by half without deteriorating the performance [33], [34]. Both of them can be fabricated using the printed circuit board (PCB) process and have many advantageous features such as low cost and easy integration with other circuits.

Before going to the detailed applications, one important problem which we should pay attention to is the feeding issue. The feeding of power into the waveguide can be troublesome since the wave is evanescent particularly in the case where the operating frequency is well below the cutoff. The way to use another large waveguide for excitation could lead to an abrupt change in the waveguide cross-section causing substantial mismatch [14], [15]. Additional stub-tuners may be required for better matching [14]. When direct coaxial probe is adopted to feed the waveguide, it has to be very close to the metamaterial loadings in order to enhance the coupling. This problem can be alleviated a little on the SIW platform [27]. A taper line between the input microstrip line and SIW can be used to match the real part and the imaginary part can be matched by tuning the waveguide length between the microstrip taper line and the metamaterial loadings. These techniques can be easily realized using the PCB technology.

Guided Wave Applications

Waveguide Miniaturization

It is well known that the transversal width of the traditional TE_{10} waveguide must be at least a half-wavelength at the cutoff frequency in the filling material, through which the field distribution can satisfy the boundary conditions needed for wave propagation along the waveguide. By filling either μ-negative or ε-negative metamaterials, the transversal width of this TE_{10}-mode based waveguide can be arbitrarily smaller than half of a wavelength in the filling material at the original cutoff frequency. This peculiar behavior has been used for fabrication of miniaturized rectangular waveguides. Figure 7 shows several miniaturization examples from the literature. The first one shown in Figure 7(a) uses the SRR arrays as a μ-negative material inserted in the waveguide

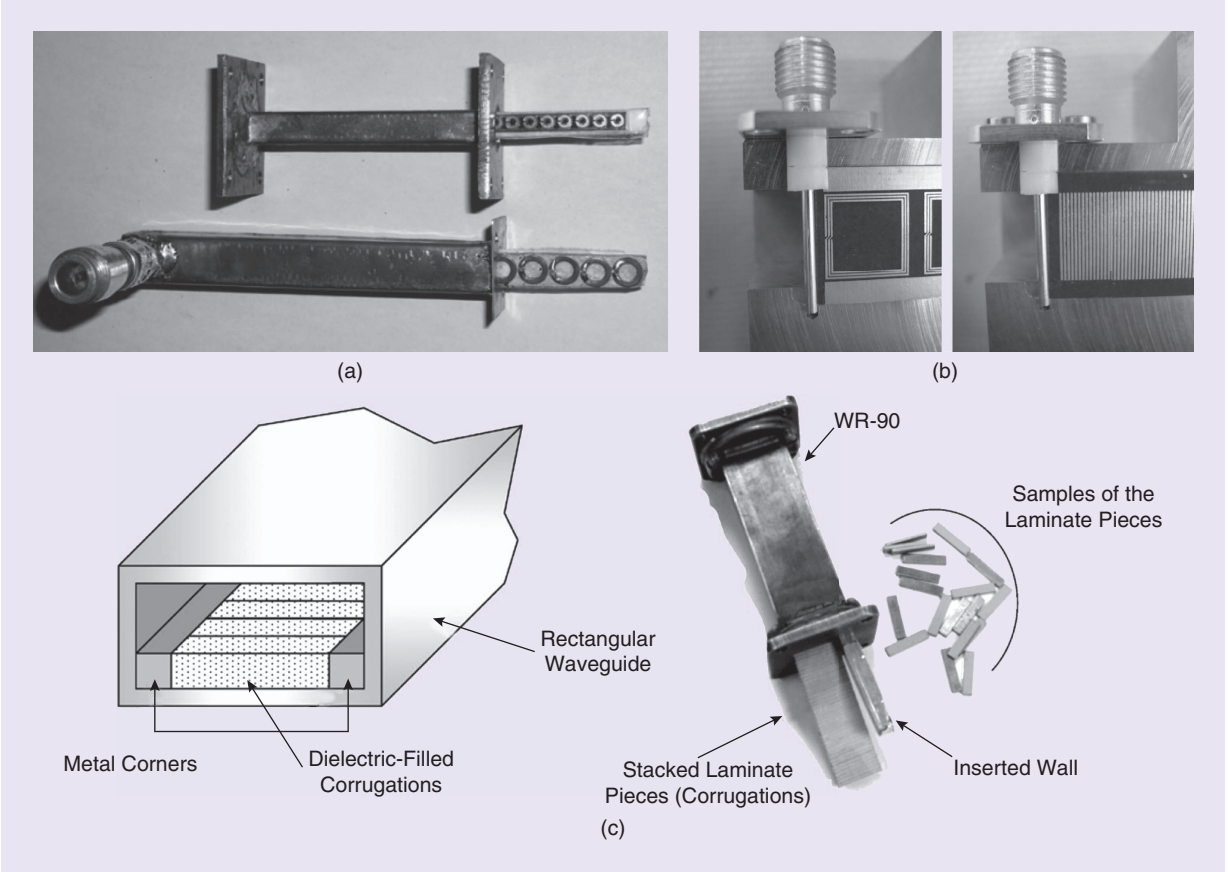

Figure 7. *Metamaterial-based waveguide miniaturization examples. (a) Waveguide loaded by SRR arrays [15], (b) waveguide loaded by spiral arrays (left) and wire dipoles (right) [26], and (c) waveguide loaded by dielectric-filled corrugations [32].*

Radiation loss can be minimized by decreasing the slot width and reducing the effective length (while the capacitance value can be kept the same).

for miniaturization [15]. The second one shown in Figure 7(b) employs the spiral resonators and dipole arrays for the purpose of waveguide miniaturization [29]. Spiral resonator essentially functions in the same way as the SRR which is able to provide negative permeability, while the wire dipole array is believed to exhibit negative permittivity which also enables wave propagation below the waveguide cutoff. Figure 7(c) demonstrates the possibility of using dielectric-filled corrugation for waveguide miniaturization [35]. The corrugation works similarly to the slot dipole which provides an LH capacitance leading to a metamaterial TL supporting wave propagation below the cutoff frequency.

Figure 8 shows the case of using interdigital slots etched on the waveguide surface to miniaturize the waveguide [36]. The introduction of slot dipoles on the SIW surface allows the implementation of a CRLH metamaterial TL. Both the full-mode and half-mode SIW cases have been studied to load the slot dipoles (interdigital capacitor), in order to realize the CRLH

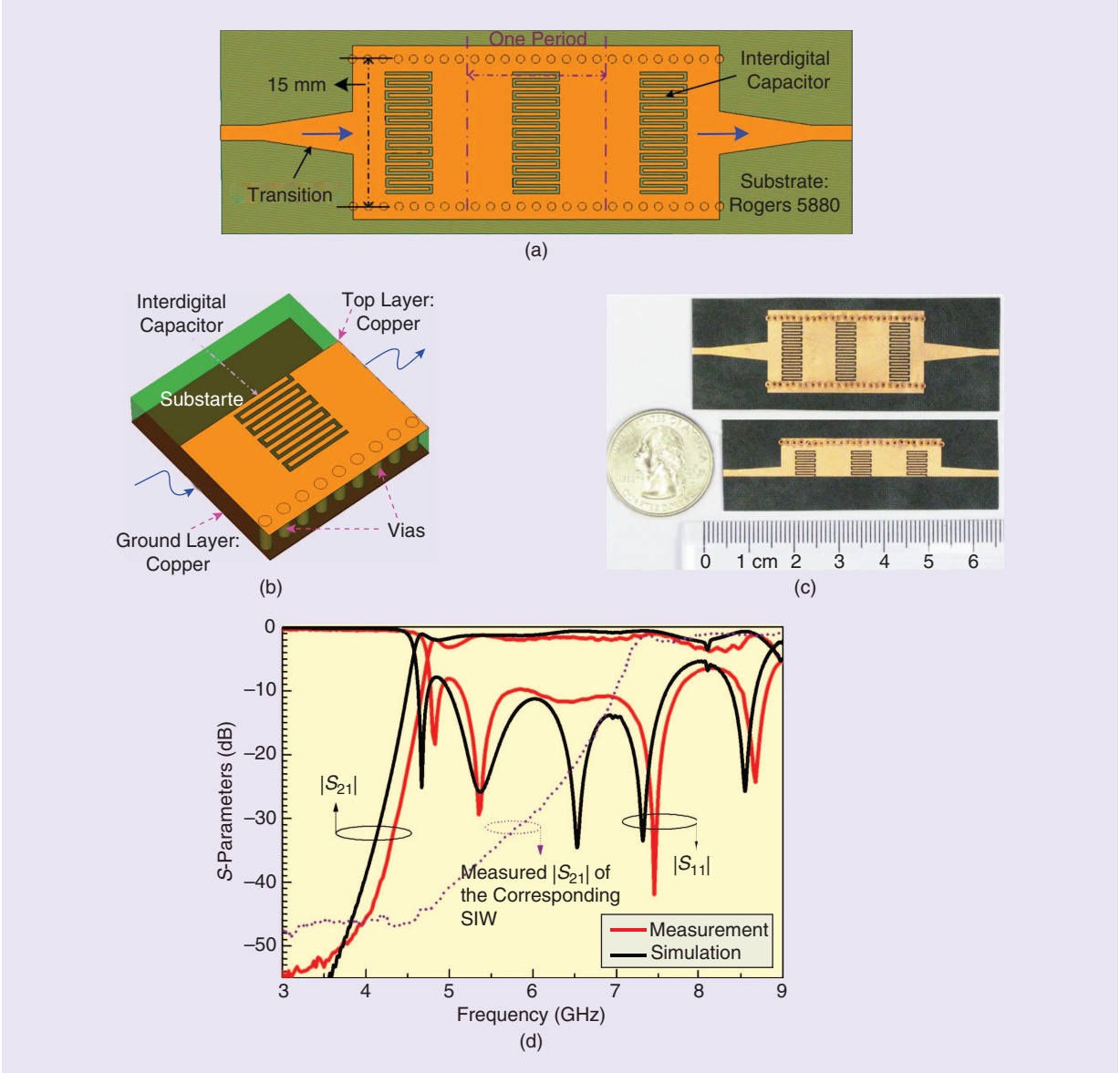

Figure 8. *The miniaturization of SIW by loading interdigital slot on the waveguide surface [33]. (a) Three-cell SIW model, (b) half-mode unit-cell configuration, (c) fabricated CRLH SIW and half-mode SIW TLs, and (d) measured and simulated transmission response of the CRLH SIW TL, which is compared with the unloaded case.*

TL. Balanced condition is achieved to integrate the LH and RH regions seamlessly so that the passband seems to be extended to a lower frequency only. Figure 8(d) shows the measured *S*-parameters for the full-mode CRLH SIW TL, which is compared with the original SIW cutoff frequency. Miniaturization is obviously obtained. It is noted that radiation loss can be minimized by decreasing the slot width and reducing the effective length (while the capacitance value can be kept the same).

Novel Coupler Design

Figure 9 shows a 3-dB backward directional coupler application [36]. It is organized by two pieces of CRLH half-mode SIW TL placed symmetrically along the open side with a small gap. Normally HMSIW TLs with similar configurations can only provide weak coupling. Here this coupler is operated in its LH region. Figure 9(c) presents the measured transmission response of the coupler. Clearly backward wave coupling is achieved. The electric field distribution at the operating frequency is plotted in Figure 9(b). Only three stages are used here to realize a 3-dB coupler. By adopting more stages, arbitrary coupling is expected to be obtained. It is noted that outside the LH region the structure is considered to be lossy.

Their center frequency and bandwidth can be adjusted by engineering the dispersion curve.

Figure 10 shows a dual-band rat-race coupler implemented with the CRLH half-mode SIW technology [37]. It has a ring-type configuration composed of six unit cells with four ports. Since the CRLH TL section is able to provide −90° and +90° phase shifts at two different frequencies as indicated by Figure 10(c), dual-band operation can be easily achieved. Their center frequency and bandwidth can be adjusted by engineering the dispersion curve. Either 180°-out-of-phase and in-phase operations can be obtained depending on the excitation port. Figure 10(d) shows the operating principle. The measured results for the 180°-out-of-phase are displayed in Figure 10(e) and (f). It is found that good matching and isolation, small amplitude imbalance are achieved at the two desired bands. Excellent 180° phase difference has also been demonstrated.

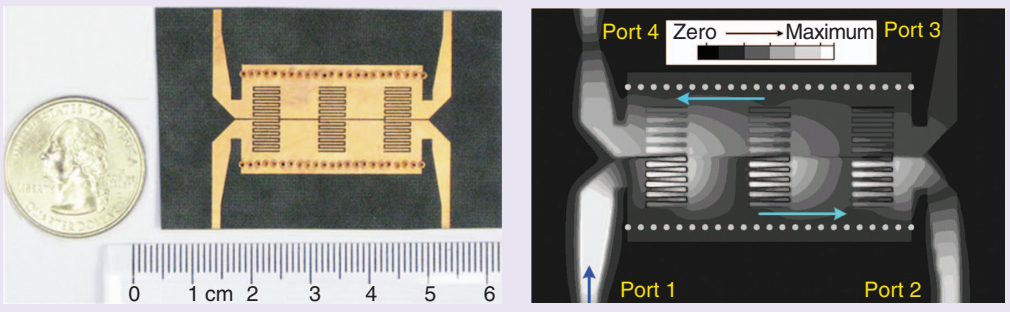

(a)

(b)

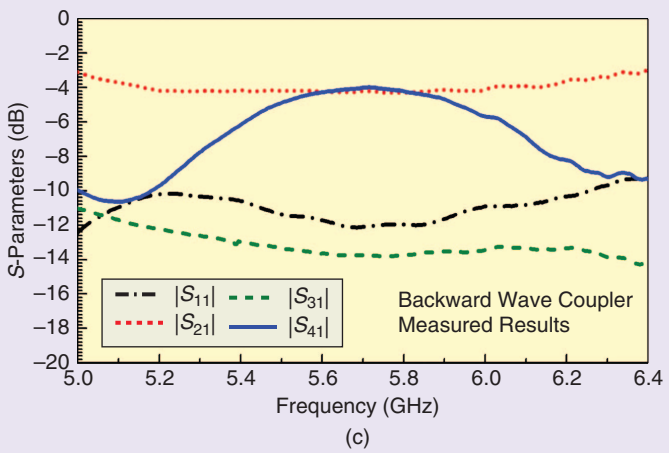

(c)

Figure 9. *Backward-wave directional coupler based on CRLH half-mode SIW TL [33]. (a) Photograph of the fabricated component, (b) electric field distribution, and (c) measured S-parameters.*

Both the SRR-loaded and CSRR-loaded waveguide structures can be used for filter applications since both of them are able to provide a high-Q passband below the cutoff frequency.

Filter Design

Both the SRR-loaded and CSRR-loaded waveguide structures can be used for filter applications since both of them are able to provide a high-Q passband below the cutoff frequency. However, it is expensive and difficult to fabricate the SRR-loaded waveguide structures. On the other hand, we can use the SIW technology to easily realize the CSRR-loaded waveguide structures at a lower cost by virtue of a planar structure.

Figure 11 shows a bandpass filter with 3 poles based on the CSRR-loaded SIW structure fabricated on the Rogers 5880 substrate with a thickness of 20-mil [23]. Three pairs of CSRR resonators are face-to-face oriented and the size of the middle pair is scaled up a little in order to adjust the resonance frequency. This filter has a passband located at 5.05 GHz, which is far below the waveguide cutoff frequency (10 GHz), and a 3-dB bandwidth of 0.33 GHz. Due to the existence of the transmission zeros, this filter exhibits a good selectivity and a stopband rejection better

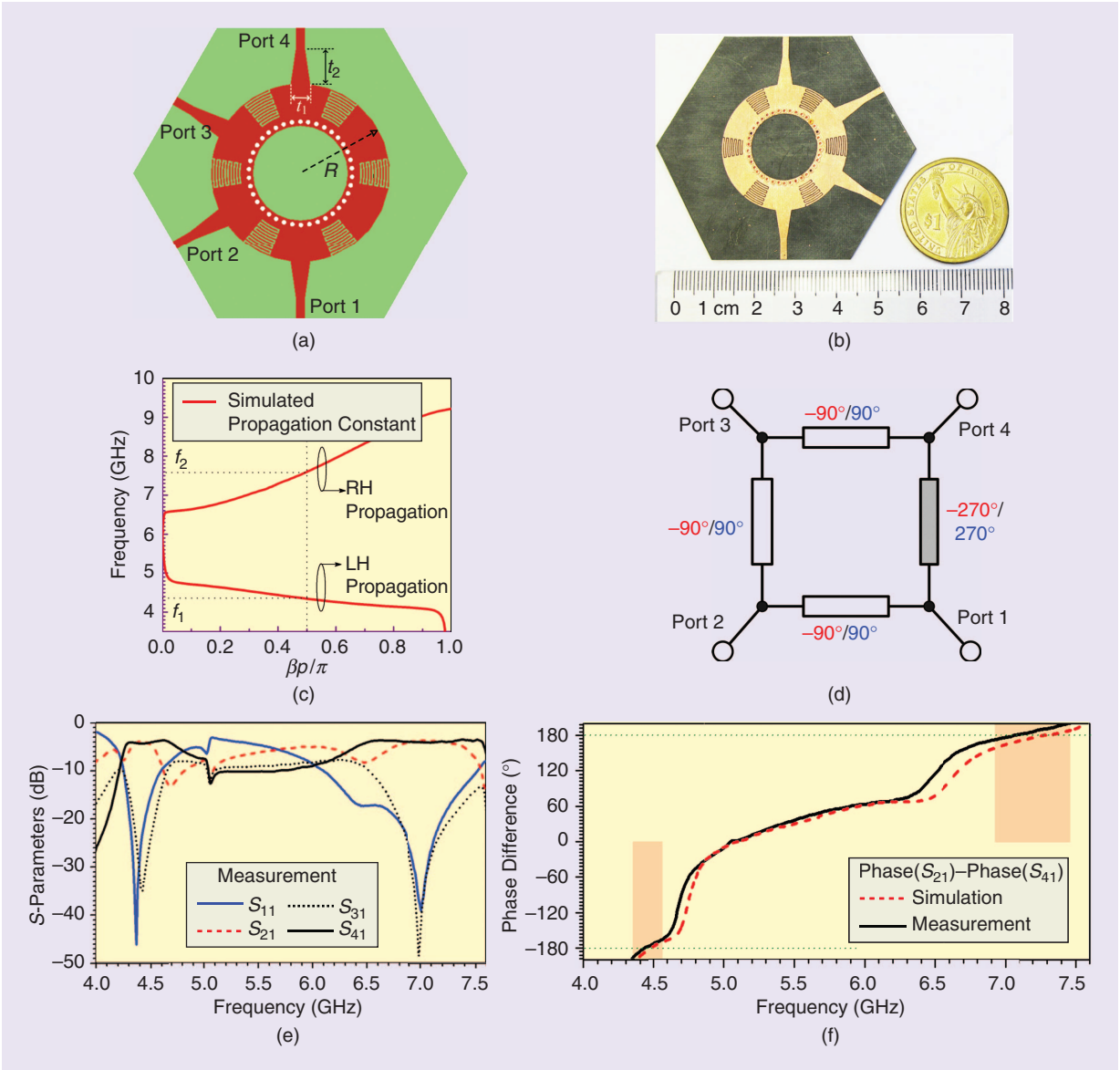

Figure 10. *Dual-band rat-race coupler based on the CRLH hall-mode SIW TLs [37]. (a) Coupler configuration, (b) photograph, (c) unit-cell dispersion diagram, (d) coupler working principle, (e) measured coupler S-parameters for out-of-phase excitation, and (f) measured phase response for out-of-phase excitation.*

than 52 dB, as observed from the measured results shown in Figure 11(b). It is noted that, since the wave is evanescent, the waveguide length between the CSRRs actually determines the internal coupling, while the waveguide length between CSRR and input microstrip line determines the external coupling. The filter size is miniaturized in terms of both the transversal dimension and the longitudinal size. Overall the proposed filter exhibits a quite good performance and a compact size due to the employment of the metamaterial or sub-wavelength resonators. Compared with other CSRR filters, such as the one using CPW technology shown in [38], our proposed filter exhibits superior performance due to the use of a high-Q waveguide format.

Figure 12 shows a two-pole dual-band filter achieved by two different types of CSRRs which are etched on the surface of the SIW structure [39]. The CSRRs are face-to-face oriented in terms of the split direction. The two CSRRs offer two relatively independent resonance frequencies where the large one corresponds to the lower frequency. A two-pole filter is constructed by arranging two resonators in a centrosymmetric way. To individually control the coupling coefficient, the configuration of the CSRRs can be adjusted instead of using the square shape [39]. Figure 12(c) shows the measured and simulated results for the designed two-pole filter. The two passbands are located at 4.05 GHz and 5.8 GHz. The total filter size is $0.199\ \lambda_0 \times 0.187\ \lambda_0 \times 0.007\ \lambda_0$, where λ_0 is the free space wavelength at the lower passband. Good filtering response is achieved. Note that both the location and bandwidth of this dual-band filter can be adjusted [39]. It is also observed that each of the two passbands is followed by two transmission zeros which greatly improves the selectivity and out-of-band rejection. Multiband filters can also be realized using the similar operating scheme.

Figure 13 shows a high-performance planar diplexer developed based on the SIW structure with CSRRs etched on the waveguide surface [40]. The proposed diplexer is operated below the characteristic cutoff frequency of the waveguide. Note that the CSRRs in this case are side-by-side reversely oriented and the middle strip is removed in order to suppress the propagation of TE_{10} mode [23]. The device performance, as demonstrated by its measured insertion loss (approximately 1.60 dB and 2.30 dB in the two bands), return loss (RL > 12.9 dB), and isolation (better than 30 dB), is good. High selectivity and improved out-of-band rejection are obtained with the help of transmission zeros and the suppression of TE_{10} mode. Compact dimension is also achieved due to the employment of the sub-wavelength resonators.

In general, the waveguide structures can be combined with the SRRs, CSRRs flexibly and applied

The filter size is miniaturized in terms of both the transversal dimension and the longitudinal size.

for filter realization. Usually these filters are operated below the waveguide cutoff frequency and exhibit a very compact size, as demonstrated by the above cases. But their applications are not limited

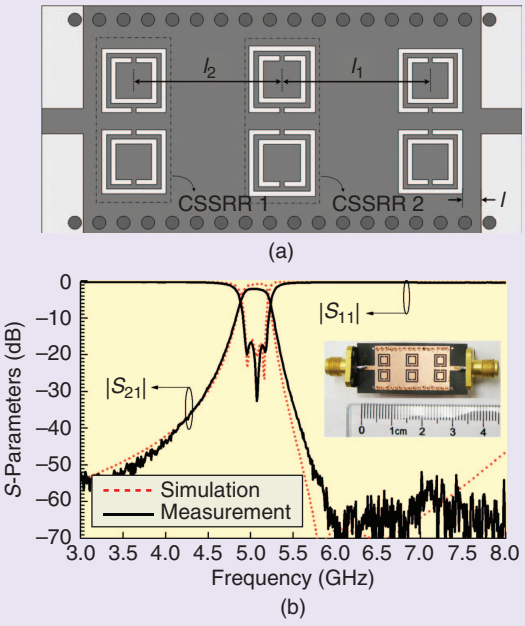

Figure 11. *CSRR-loaded SIW three-pole filter [22]. (a) Filter configuration and (b) simulated and measured filter response with a photograph shown in the inset.*

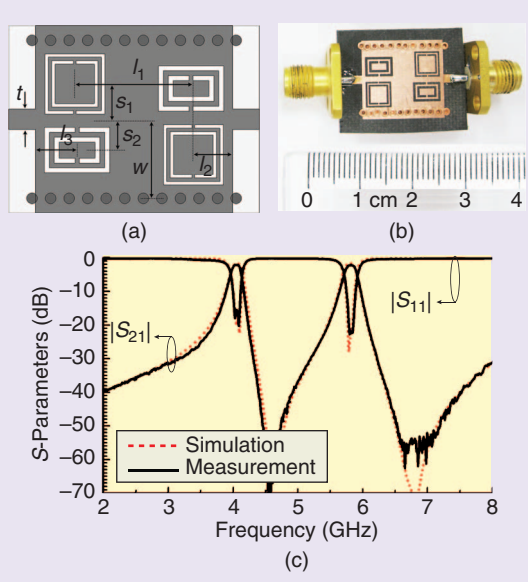

Figure 12. *Single-ring CSRR-SIW dual-band filter [39]. (a) Filter structure, (b) photograph, and (c) simulated and measured filtering response.*

to these bandpass filters. By operating the SRR and CSRR metamaterial elements above the waveguide cutoff frequency, single negative (either μ-negative or ε-negative) metamaterial can be obtained which can be used to design bandstop filters. One illustrative example is shown in Figure 14, where a multiband bandstop filter was developed [41].

Radiated Wave Applications

Resonator-Type Antennas

The structure shown in Figure 6 where the waveguide is loaded by slot dipole can be used to construct the negative order resonance antennas. Figure 15 shows a family of the SIW negative order

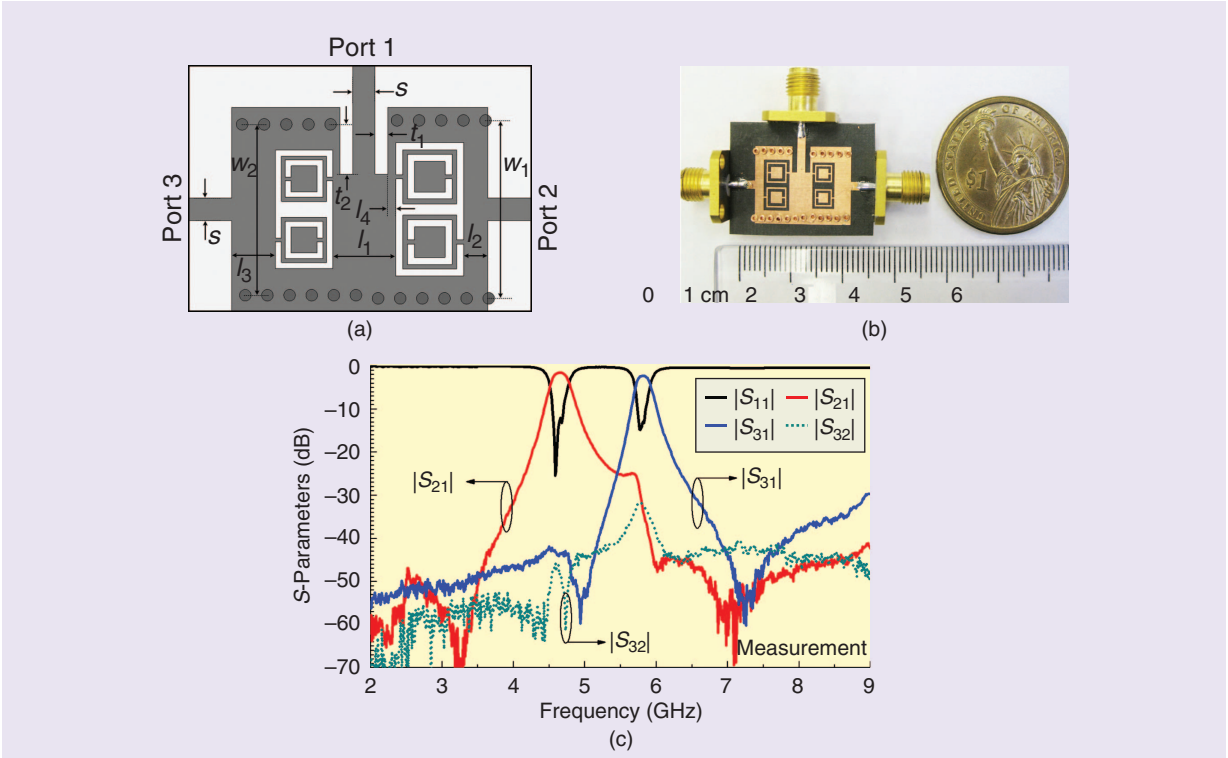

Figure 13. *Miniaturized diplexer based on the CSRR-SIW structure [40]. (a) Diplexer configuration, (b) photograph, and (c) measured S-parameters.*

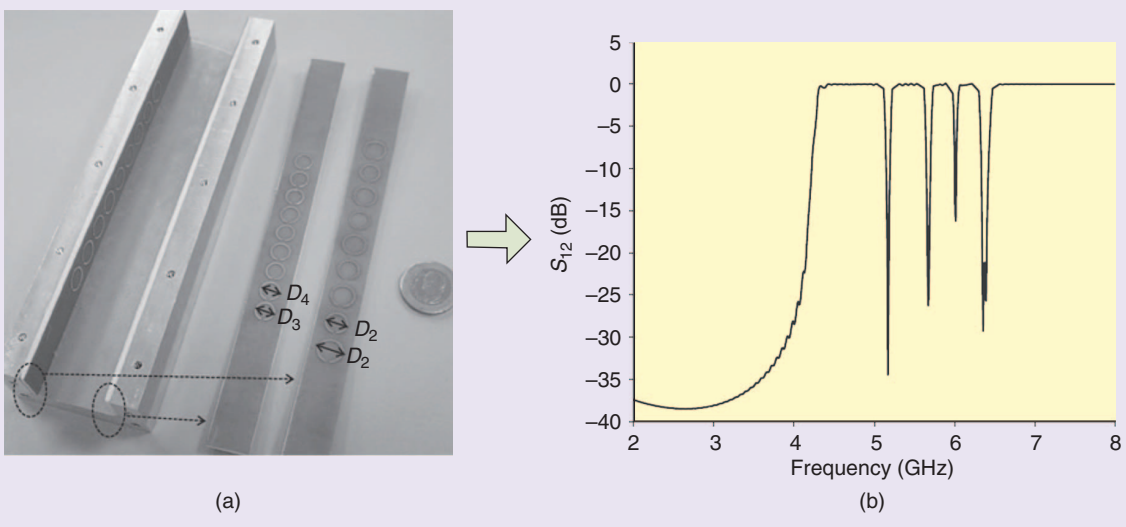

Figure 14. *Multistopband filters by SRR-loaded waveguide proposed in [41]. (a) Filter structure and (b) simulated filtering response.*

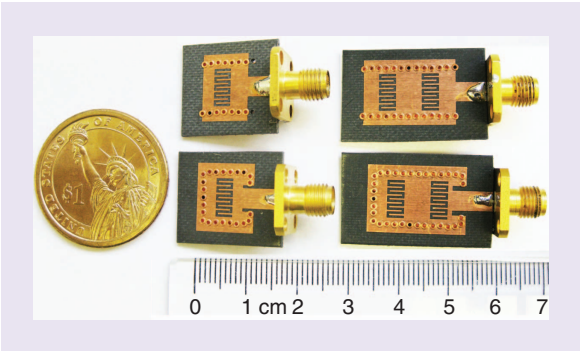

Figure 15. *Fabricated CRLH SIW slot antennas based on the negative order mode [38].*

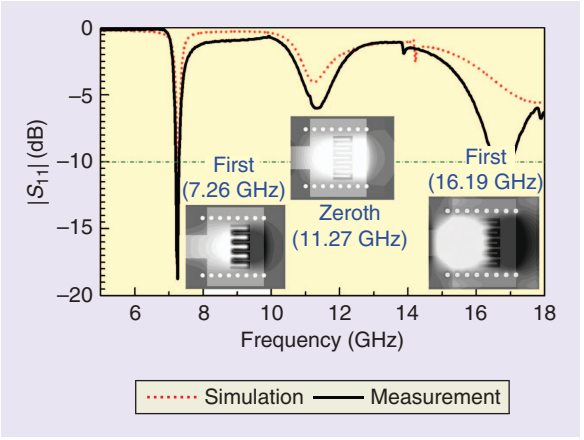

Figure 16. *Reflection coefficient and field distribution of the CRLH SIW open-ended antenna. The antenna works on the -1st mode [38].*

resonance antennas [42]. By introducing the interdigital slots on the waveguide surface, a CRLH resonator-type structure can be realized and negative order resonances can be created. These antennas are operated on −1st mode whose resonance frequency is far below the original waveguide cutoff frequency. Unbalanced condition is usually selected in order to push down the LH region for miniaturization. Figure 16 shows the simulated and measured reflection coefficient for the one-stage open-ended antenna. The electric field distribution at three different resonance frequencies (−1st, 0th, and 1st) is also plotted in the inset of the figure. The cutoff frequency of the corresponding SIW TL is at 11.3 GHz. A significant degree of miniaturization is achieved by an LH region operation. It is also seen that the −1st mode is actually very similar to the 1st mode in terms of the field distribution, both of which appear as a half-wavelength resonator. This antenna is very suitable for multiband application by using different resonance simultaneously.

We can also design a quarter-wavelength resonator for the resonator-type slot antenna [42]. This is achieved by closing the boundary and moving the outside boundary close to the center as indicated by Figure 17(a). This is because the center of the half-wavelength slot antenna always has zero voltage. A cavity-backed slot antenna is created. Under this configuration the −1st order resonance switches to a quasi-quarter-wavelength resonator and the zeroth-order resonance is eliminated since

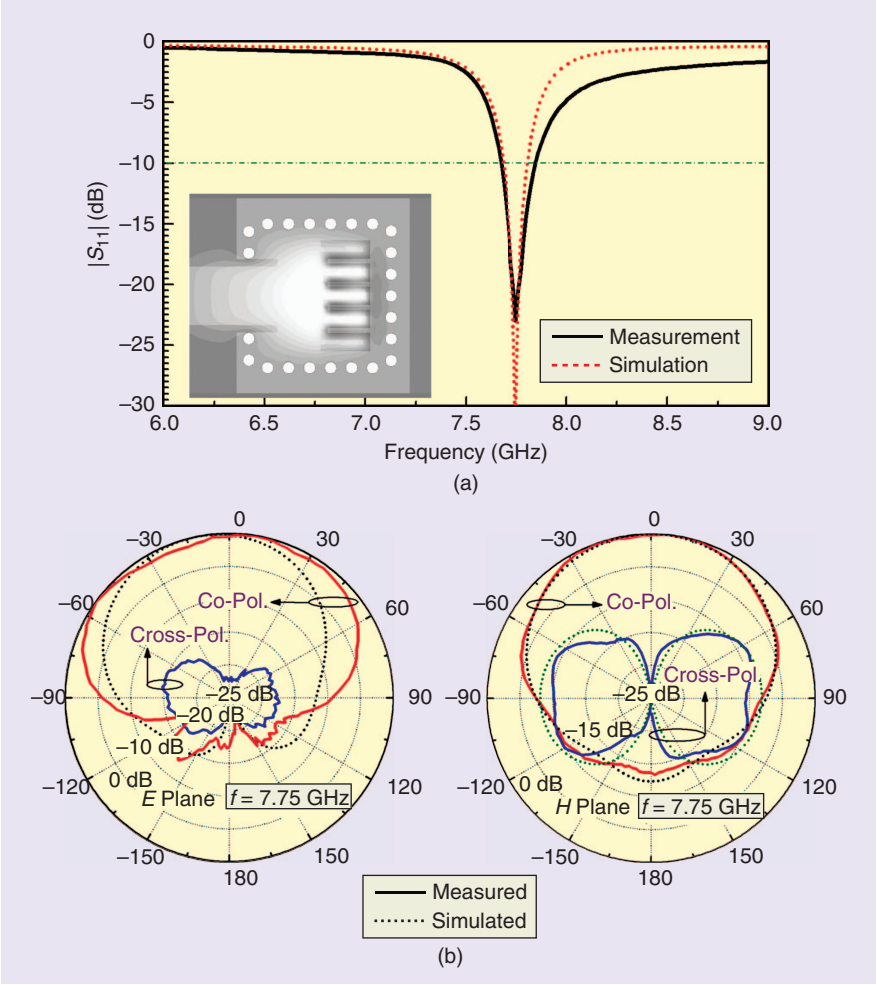

Figure 17. *(a) Reflection coefficient, filed distribution and (b) radiation patterns in E-plane and H-plane for the short-ended CRLH-SIW slot antenna. This antenna also works on the -1st mode [42].*

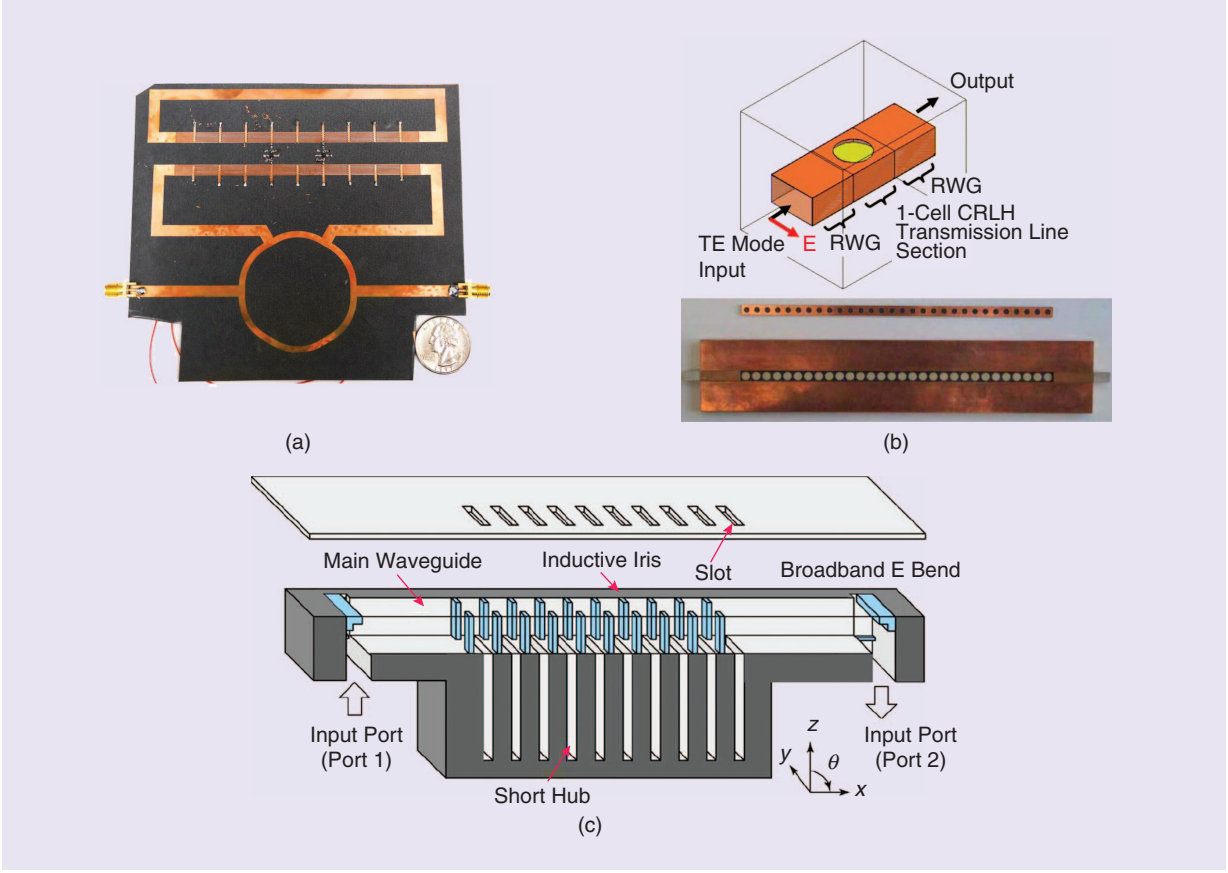

Figure 18. *(a) Gain-enhanced distributed amplifier-based CRLH leaky wave antenna based on a power recycling feedback scheme [40], (b) unit-cell configuration and photograph of the dielectric resonator based CRLH waveguide leaky-wave antennas [27], and (c) a stub-loaded LH waveguide slot array leaky-wave antenna [41].*

the uniform field is forced to be zero by the boundary condition. Figure 17 shows the measured and simulated reflection coefficient and radiation patterns for this short-ended antenna. The −1st order mode is clearly observed and its resonance frequency is around 7.75 GHz. The radiation pattern is very similar to the pattern of a patch antenna. This antenna has a radiation efficiency of 91% in the simulation and 87% in the measurement. The good efficiency can be attributed to the cavity-backed configuration and a waveguide-type operation mode.

Leaky-Wave Antennas

Conventional CRLH leaky-wave antennas in microstrip format is usually lossy therefore inefficient. One way to improve the efficiency is to use the active circuit and power-recycling scheme to increase the radiation efficiency [43], [44]. One illustrative example is shown in

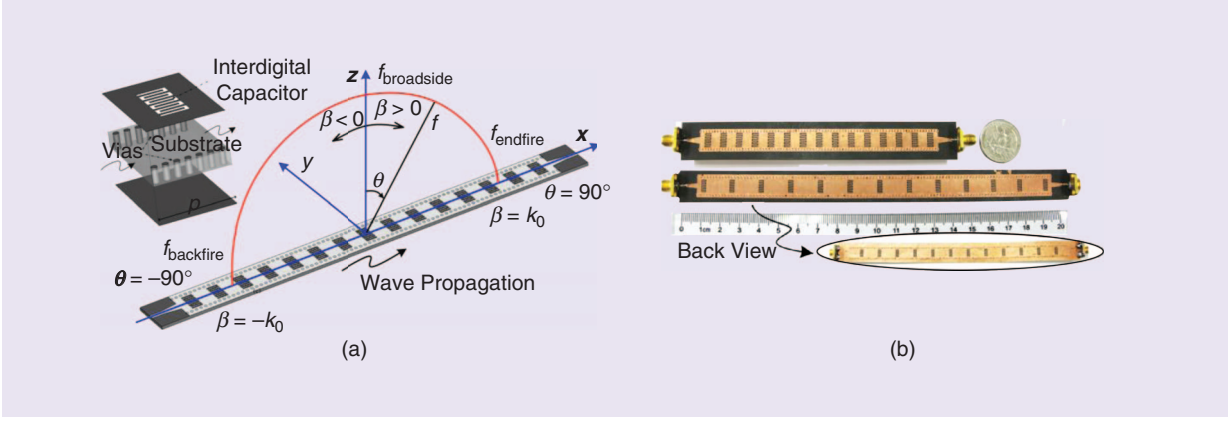

Figure 19. *(a) The detailed structure and (b) photograph of the CRLH SIW leaky-wave antennas [24].*

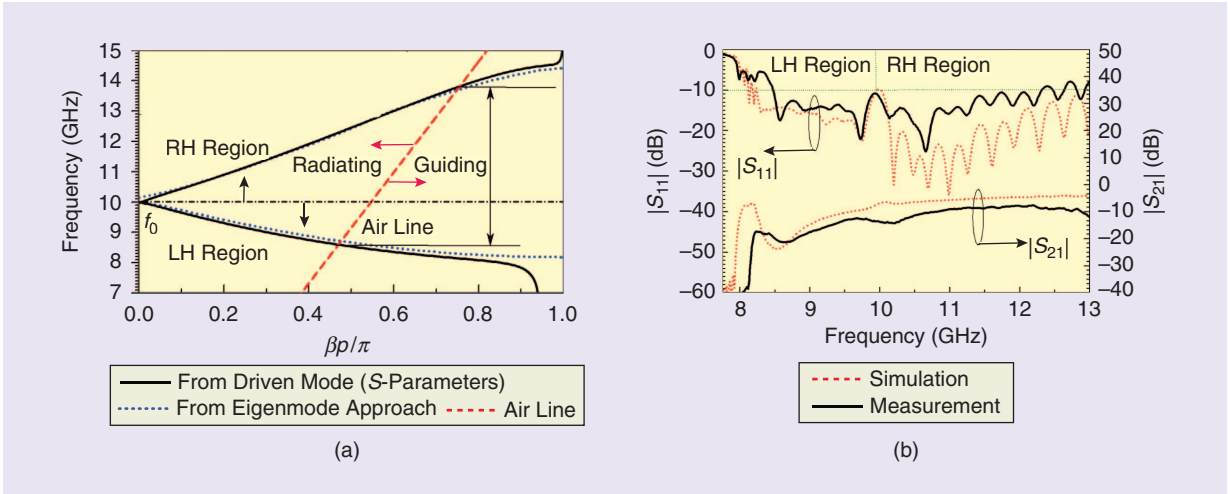

Figure 20. *(a) The unit-cell dispersion diagram and (b) the simulated and measured S-parameters of the single-side CRLH SIW leaky-wave antenna [24].*

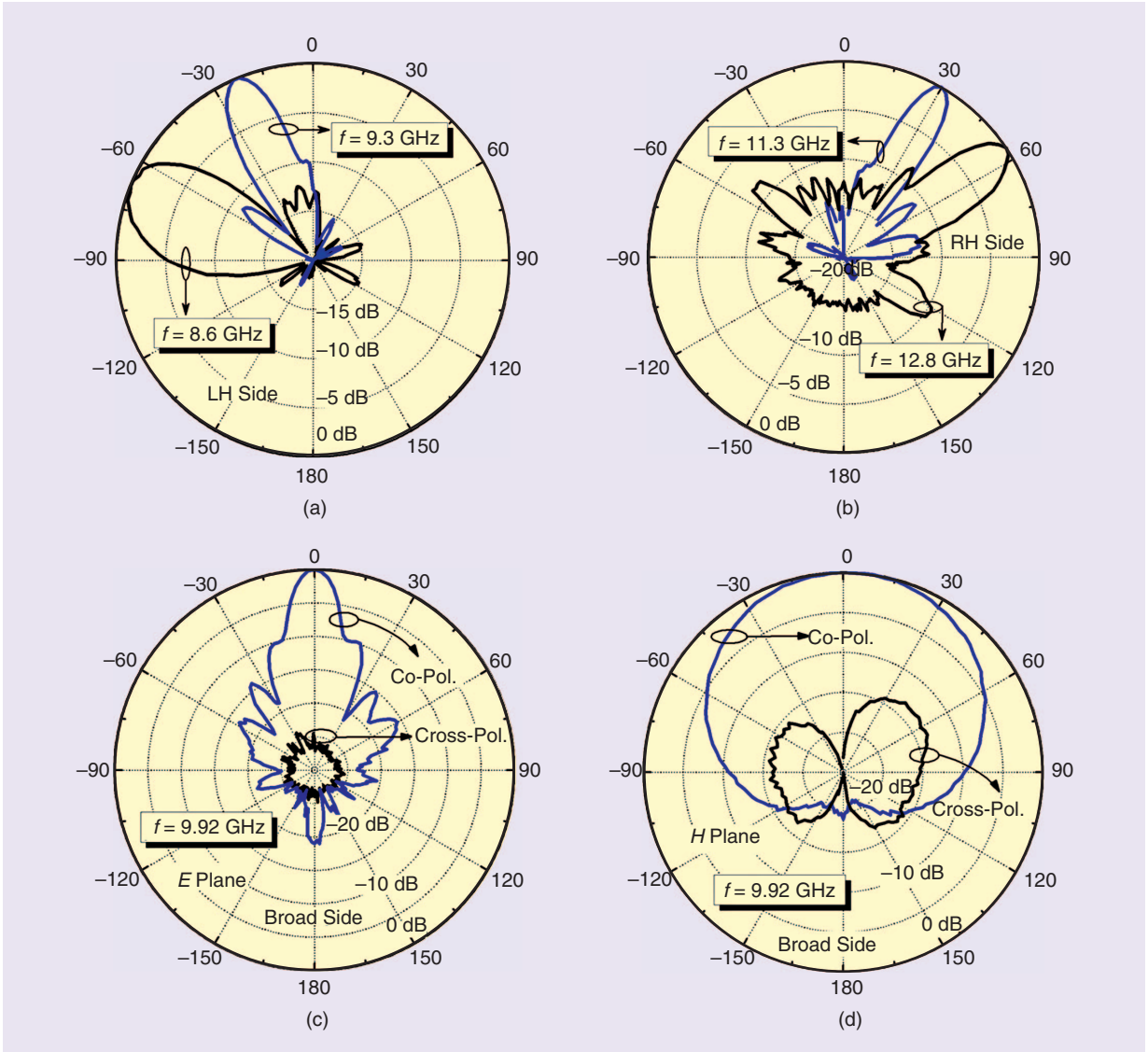

Figure 21. *Measured radiation patterns of the single-side CRLH SIW leaky-wave antenna (a) in the LH region, (b) in the RH region, (c) E-plane pattern, and (d) H-plane pattern at the transition frequency [24].*

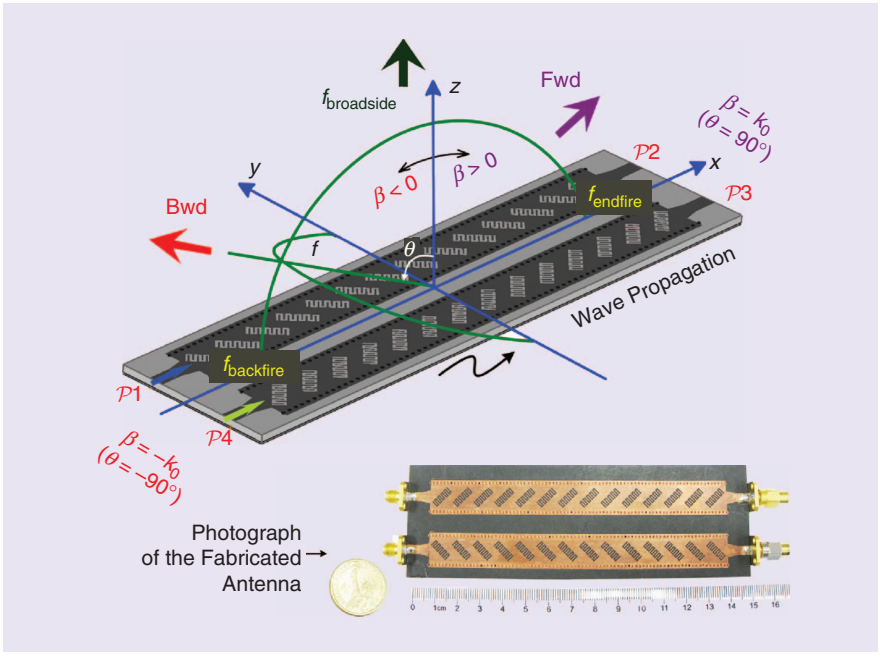

Figure 22. *The overall structure and photograph of the fabricated polarization-flexible leaky-wave antenna [43].*

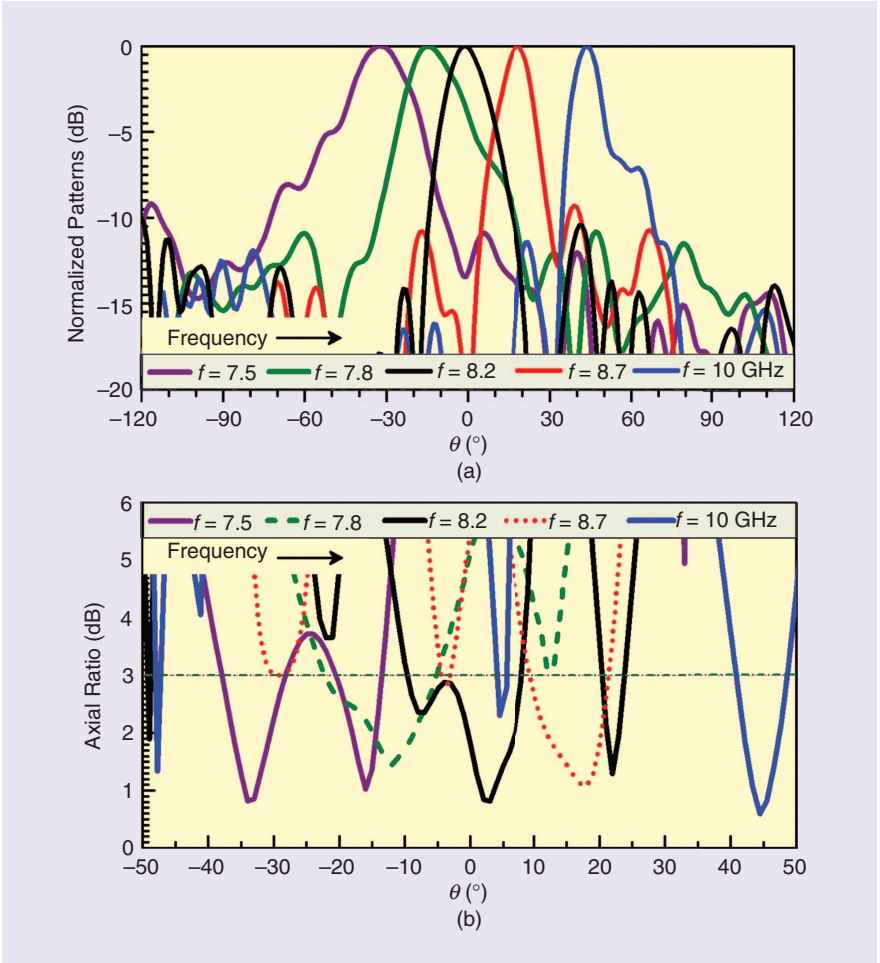

Figure 23. *Measured (a) radiation patterns and (b) axial ratio for the CP case of the polarization-flexible leaky-wave antenna. Backward (LH region) to forward (RH region) continuous beam scanning with a good CP mode inside the main beam is observed [43].*

Figure 18(a), where a gain-enhanced power recycling feedback is employed for distributed amplifier-based CRLH leaky-wave antenna application [44]. Another approach is to switch to waveguide structures. There are already several waveguide-based CRLH leaky-wave antennas that have been proposed, such as the dielectric resonator based CRLH waveguide leaky-wave antenna shown in Figure 18(b) [30], and the stub-loaded LH waveguide slot array leaky-wave antenna displayed in Figure 18(c) [45].

However, those metamaterial leaky-wave waveguide antennas are relatively complicated. The unit-cell shown in Figure 6 can be employed for leaky-wave antenna applications. We can increase interdigital slot width and increase the length to allow more radiation while keeping the LH capacitance value unchanged. Figure 19 shows the designed unit-cell, antenna structure and the photograph of the fabricated SIW leaky-wave antennas [27]. Note that the slot can be either etched on one side or two sides to generate quasi-omnidirectional radiation. Figure 20 shows the dispersion diagram of the unit-cell and measured *S*-parameters of the single-side leaky-wave antenna. The dispersion curve shows that the radiating region corresponds to the area on the left side of the airline. The LH and RH regions are separated by the transition frequency. Thanks to a balanced design, backward, broadside and forward continuous beam scanning is achieved which is verified by radiation pattern shown in Figure 21. An average radiation efficiency of 82% is reported for this leaky-wave

antenna. Half-mode CRLH SIW antennas have also been proposed and investigated in [27].

We can also modify the proposed CRLH SIW leaky structure to achieve some interesting functions. A CRLH leaky-wave structure for polarization-flexible antenna application is proposed in [46], [47]. The antenna structure is shown in Figure 22. It consists of two symmetrical waveguide TLs loaded with series interdigital slots which are rotated and radiate orthogonal 45° linearly polarized waves. It is able to generate arbitrarily different polarization states by changing the way of excitation including linear polarization (LP) and circular polarization (CP). Six different polarization states, including four LP cases and two CP ones, have been experimentally verified in [47]. Figure 23 shows the measured radiation patterns and axial ratio for the CP case. Note that a broad band 90° directional coupler is used in this case. It is seen that the main beam of this antenna can be steered continuously by varying the frequency while maintaining a low axial ratio (below 3 dB) within the main beam direction. This leaky-wave antenna shows some desirable merits such as the simplicity in design, low-cost in fabrication, beam-steering and polarization-flexible capabilities, providing a high degree of flexibility for the real application.

Conclusion

This article summarized and reviewed the realization and applications of the waveguide-based metamaterial structures. In particular, an overview of the existing metamaterial elements was presented. We discussed the possible solutions to enable wave propagation below the waveguide cutoff frequency by loading these elements. Then a detailed analysis on those waveguide unit-cells loaded with different metamaterial elements was provided based on HFSS simulation. Various guided and radiated microwave applications based on these novel metamaterial-based waveguide structures were presented. Those obtained simulation and experimental results were found to be in good agreement with the theoretical prediction. These applications also demonstrate that the combination of waveguide structure and metamateials offers an excellent alternative approach to the design of miniaturized and high-performance microwave components. Waveguide has high-power handling capability and high Q-factor. It also provides a uniform and lossless ε-negative (μ-negative) environment when operated based on the TE modes (TM modes) below the cutoff frequency. This is a promising and potentially rewarding research topic. We are looking forward to achieving more truly high-performance metamaterial devices by taking advantages of these features in the near future.

The combination of waveguide structure and metamateials offers an excellent alternative approach to the design of miniaturized and high-performance microwave components.

References

[1] R. A. Shelby, D. R. Smith, and S. Schultz, "Experimental verification of a negative index of refraction," *Science*, vol. 292, no. 5514, pp. 77–79, 2001.

[2] C. Caloz and T. Itoh, *Electromagnetic Metamaterials: Transmission Line Theory and Microwave Applications*. New York: Wiley-IEEE Press, 2005.

[3] G. V. Eleftheriades and K. G. Balmain, *Negative Refraction Metamaterials: Fundamental Principles and Applications*. New York: Wiley-IEEE Press, 2005.

[4] N. Engheta and R. W. Ziolkowski, *Electromagnetic Metamaterials: Physics and Engineering Explorations*. New York, Wiley-IEEE Press, 2006.

[5] R. Marques, F. Martin, and M. Sorolla, *Metamaterials with Negative Parameters: Theory, Design and Microwave Applications*. Hoboken, NJ: Wiley, 2008.

[6] T. J. Cui, R. Liu, and D. R. Smith, *Metamaterials: Theory, Design and Applications*. New York: Springer-Verlag, 2010.

[7] A. Lai, C. Caloz, and T. Itoh, "Composite right/left-handed transmission line metamaterials," *IEEE Microwave Mag.*, vol. 5, no. 3, pp. 34–50, Sept. 2004.

[8] A. Lai, K. Leong, and T. Itoh, "Infinite wavelength resonant antennas with monopolar radiation pattern based on periodic structures," *IEEE Trans. Antennas Propagat.*, vol. 55, no. 3, pp. 868–876, Mar. 2007.

[9] M. Antoniades, and G. V. Eleftheriades, "A folded-monopole model for electrically small NRI-TL metamaterial antennas," *IEEE Antennas Wireless Propagat. Lett.*, vol. 7, pp. 425–428, 2008.

[10] J. B. Pendry, A. J. Holden, D. J. Robbins, and W. J. Stewart, "Magnetism from conductors and enhanced nonlinear phenomena," *IEEE Trans. Microwave Theory Tech.*, vol. 47, no. 11, pp. 2075–2084, Nov. 1999.

[11] J. D. Baena, J. Bonache, F. Martin, R. Marques, F. Falcone, T. Lopetegi, M. Laso, J. Garcia, I. Gil, M. F. Portillo, and M. Sorolla, "Equivalent-circuit models for split-ring resonators and complementary split-ring resonators coupled to planar transmission lines," *IEEE Trans. Microwave Theory Tech.*, vol. 53, no. 4, pp. 1451–1461, Apr. 2005.

[12] F. Falcone, T. Lopetegi, J. D. Baena, R. Marques, F. Martin, and M. Sorolla, "Effective negative-epsilon stopband microstrip lines based on complementary split ring resonators," *IEEE Microwave Wireless Comp. Lett.*, vol. 14, no. 14, pp. 280–282, June 2004.

[13] G. V. Eleftheriades, A. K. Iyer, and P. C. Kremer, "Planar negative refractive index media using periodically L-C loaded transmission lines," *IEEE Trans. Microwave Theory Tech.*, vol. 50, pp. 2702–2712, Dec. 2002.

[14] R. Marques, J. Martel, F. Mesa, and F. Medina, "Left-handed-media simulation and transmission of EM waves in subwavelength split ring resonator-loaded metallic waveguides," *Phys. Rev. Lett.*, vol. 89, no. 18, pp. 183901–183904, Oct. 2002.

[15] S. Hrabar, J. Bartolic, and Z. Sipus, "Waveguide miniaturization using uniaxial negative permeability metamaterial," *IEEE Trans. Antennas Propagat.*, vol. 53, no. 1, pp. 110–119, Jan. 2005.

[16] J. Esteban, C. C. Penalosa, J. E. Page, T. M. Martin-Guerrero, and E. Marquez-Segura, "Simulation of negative permittivity and negative permeability by means of evanescent waveguide modes—Theory and experiment," *IEEE Trans. Microwave Theory Tech.*, vol. 53, no. 4, pp. 1506–1514, Apr. 2005.

[17] P. Belov and C. Simovski, "Subwavelength metallic waveguides loaded by uniaxial resonant scatterers," *Phys. Rev. E*, vol. 72, pp. 0366181–03661811, Sept. 2005.

[18] Q. Zhang, S. N. Khan, and S. He, "Realization of left handedness through CSRRs and SRRs in microstrip line," *Microwave Opt. Technol. Lett.*, vol. 51, no. 3, pp. 757–760, Mar. 2009.

[19] D. Sievenpiper, L. Zhang, F. J. Broas, N. G. Alexopulos, and E. Yablonovitch, "High-impedance electromagnetic surfaces with a forbidden frequency band," *IEEE Trans. Microwave Theory Tech.*, vol. 47, pp. 2059–2074, Nov. 1999.

[20] A. Sanada, C. Caloz, and T. Itoh, "Planar distributed structures with negative refractive properties," *IEEE Trans. Microwave Theory Tech.*, vol. 52, pp. 1252–1263, Apr. 2004.

[21] M. Gil, J. Bonache, J. Garcia, J. Martel, and F. Martin, "Composite right/left-handed metamaterial transmission lines based on complementary split-rings resonators and their applications to very wideband and compact filter design," *IEEE Trans. Microwave Theory Tech.*, vol. 55, no. 6, pp. 1296–1303, June 2007.

[22] D. M. Pozar, *Microwave Engineering*, 3rd ed. Hoboken, NJ: Wiley, 2005.

[23] Y. Dong, T. Yang, and T. Itoh, "Substrate integrated waveguide loaded by complementary split-ring resonators and its applications to miniaturized waveguide filters," *IEEE Trans. Microwave Theory Tech.*, vol. 57, no. 9, pp. 2211–2223, Sept. 2009.

[24] D. R. Smith, D. C. Vier, Th. Koschny, and C. M. Soukoulis, "Electromagnetic parameter retrieval from inhomogeneous metamaterials," *Phys. Rev. E*, vol. 71, no. 3, pp. 036617(1)–036617(11), 2005.

[25] R. V. Snyder, "New application of evanescent mode wave-guide to filter design," *IEEE Trans. Microwave Theory Tech.*, vol. 25, no. 12, pp. 1013–1021, Dec. 1977.

[26] J. Bornemann and F. Arndt, "Transverse resonance, standing wave, and resonator formulations of the ridge waveguide eigenvalue problem and its application to the design of E-plane finned waveguide filters," *IEEE Trans. Microwave Theory Tech.*, vol. 38, no. 8, pp. 1104–1113, Aug. 1990.

[27] Y. Dong and T. Itoh, "Composite right/left-handed substrate integrated waveguide and half mode substrate integrated waveguide leaky-wave structures," *IEEE Trans. Antennas Propagat.*, vol. 59, no. 3, pp. 767–775, Mar. 2011.

[28] Y. Dong and T. Itoh, "Composite right/left-handed substrate integrated waveguide leaky-wave antennas," in *Proc. European Microwave Conf.*, Rome, Italy, Sept. 2009, pp. 276–279.

[29] G. Lubkowski, C. Damm, B. Bandlow, R. Schuhmann, M. Schubler, and T. Weiland, "Waveguide miniaturization using spiral resonators and dipole arrays," in *Proc. European Microwave Conf. (EuMC)*, 2006, pp. 1312–1315.

[30] T. Ueda, N. Michishita, M. Akiyama, and T. Itoh, "Dielectric-resonator-based composite right/left-handed transmission lines and their application to leaky wave antenna," *IEEE Trans. Microwave Theory Tech.*, vol. 56, no. 10, pp. 2259–2268, Oct. 2008.

[31] J. Hirokawa and M. Ando, "Single-layer feed waveguide consisting of posts for plane TEM wave excitation in parallel plates," *IEEE Trans. Antennas Propagat.*, vol. 46, no. 5, pp. 625–630, May 1998.

[32] D. Deslandes and K.Wu, "Integrated microstrip and rectangular waveguide in planar form," *IEEE Microwave Wireless Comp. Lett.*, vol. 11, no. 2, pp. 68–70, Feb. 2001.

[33] W. Hong, B. Liu, Y. Q. Wang, Q. H. Lai, and K. Wu (invited talk), "Half mode substrate integrated waveguide: A new guided wave structure for microwave and millimeter wave application," in *Proc. Joint 31st Int. Infrared Millimeter Waves Conf./14th Int. Terahertz Electronics Conf.*, Shanghai, China, Sept. 18–22, 2006, p. 219.

[34] Y. D. Dong, W. Hong, Z. Q. Kuai, C. Yu, Y. Zhang, J. Y. Zhou, and J. Chen, "Development of ultrawideband antenna with multiple bandnotched characteristics using half mode substrate integrated waveguide cavity technology," *IEEE Trans. Antennas Propagat.*, vol. 57, no. 12, pp. 2894–2902, Sept. 2008.

[35] I. Eshrah, A. Kishk, A. Yakovlev, and A. Glisson, "Rectangular waveguide with dielectric-filled corrugations supporting backward waves," *IEEE Trans. Microwave Theory Tech.*, vol. 53, no. 11, pp. 3298–3304, Nov. 2005.

[36] Y. Dong and T. Itoh, "Composite right/left-handed substrate integrated waveguide and half-mode substrate integrated waveguide," in *IEEE MTT-S Int. Microwave Symp. Dig.*, Boston, 2009, pp. 49–52.

[37] Y. Dong and T. Itoh, "Application of composite right/left-handed half-mode substrate integrated waveguide to the design of a dual-band rat-race coupler," in *IEEE MTT-S Int. Microwave Symp.* Dig., 2010, pp. 712–715.

[38] J. Garcia, J. Bonache, I. Gil, F. Martin, M. Castillo, and J. Martel, "Miniaturized microstrip and CPW filters using coupled metamaterial resonators," *IEEE Trans. Microwave Theory Tech.*, vol. 54, no. 6, pp. 2628–2635, June 2006.

[39] Y. Dong and T. Itoh, "Miniaturized dual-band substrate integrated waveguide filters using complementary split-ring resonators," in *IEEE MTT-S Int. Microwave Symp. Dig.*, Baltimore, June 5–10, 2011, pp. 1–4.

[40] Y. Dong and T. Itoh, "Substrate integrated waveguide loaded by complementary split-ring resonators for miniaturized diplexer design," *IEEE Microwave Wireless Comp. Lett.*, vol. 21, no. 1, pp. 10–12, Jan. 2011.

[41] M. Kehn, O. Teruel, and E. Iglesias, "Split-ring resonator loaded waveguides with multiple stopbands," *Electron. Lett.*, vol. 44, no. 12, pp. 714–716, June 2008.

[42] Y. Dong and T. Itoh, "Miniaturized substrate integrated waveguide slot antennas based on negative order resonance," *IEEE Trans. Antennas Propagat.*, vol. 58, no. 12, pp. 3856–3864, Dec. 2010.

[43] H. V. Nguyen, A. Parsa, and C. Caloz, "Power-recycling feedback system for maximization of leaky-wave antennas radiation efficiency," *IEEE Trans. Microwave Theory Tech.*, vol. 58, no. 7, pp. 1641–1650, July 2009.

[44] C. T. Wu and T. Itoh, "Combined gain-enhanced power recycling feedbacks for distributed amplifier-based CRLH leaky wave antennas", in *Proc. European Microwave Conf.*, Manchester, U.K., Oct. 2011, pp. 499–502.

[45] T. Ikeda, K. Sakakibara, T. Matsui, N. Kikuma, and H. Hirayama, "Beam-scanning performance of leaky-wave slot-array antenna on variable stub-loaded left-handed waveguide," *IEEE Trans. Antennas Propagat.*, vol. 56, no. 12, pp. 3611–3618, Dec. 2008.

[46] Y. Dong and T. Itoh, "Realization of a composite right/left-handed leaky-wave antenna with circular polarization," in *Proc. Asia-Pacific Microwave Conf.*, Yokohama, Japan, Dec. 2010, pp. 865–868.

[47] Y. Dong and T. Itoh, "Substrate integrated composite right/left-handed leaky-wave structure for polarization-flexible antenna application," *IEEE Trans. Antennas Propagat.*, to be published.